Anisotropic magnetothermal resistance in Ni nanowires

Johannes Kimling,* Johannes Gooth, and Kornelius Nielsch
Institut für Angewandte Physik, Universität Hamburg, Jungiusstraße 11, D-20355 Hamburg (Germany)
(Received 15 January 2013; revised manuscript received 9 February 2013; published 8 March 2013)

We present measurements of the electrical and thermal transport properties of individual Ni nanowires as a function of the applied magnetic field, recorded in the temperature range between 78 and 380 K. In analogy to the anisotropic magnetoresistance (AMR) effect observed in ferromagnetic conductors, we find that the thermal resistance of Ni nanowires depends on the angle between magnetization vector and current direction. This anisotropic magnetothermal resistance effect turns out to be weaker than the AMR effect in Ni nanowires over the temperature range investigated. As a consequence, also the Lorenz number is found to be anisotropic with respect to the magnetization direction. To explain our observation, we propose a simple model that considers spin mixing due to electron-magnon scattering.

DOI: 10.1103/PhysRevB.87.094409 PACS number(s): 75.47.−m, 73.63.−b, 72.15.Gd

I. INTRODUCTION

In ferromagnetic metals the electrical resistivity depends on the direction of the current relative to the magnetization vector.[1] This effect is known as anisotropic magnetoresistance (AMR) and its physical origin has been ascribed to the spin-orbit interaction.[2–7] The AMR effect in ferromagnetic nanowires has been used, for example, to determine the critical fields for magnetization reversal,[8–11] or to detect magnetic domain walls.[12,13] The work of Kamalakar *et al.* focused on the electrical transport properties of Ni nanowires.[14,15] Thermal and thermoelectric transport measurements were reported for lithographically patterned thin films.[16,17] Anisotropies similar to AMR have been observed in the Seebeck coefficient of ferromagnetic nanowires[18,19] and of ferromagnetic thin films.[20] Research in the coupling of spin, charge, and heat currents in magnetic thin films and nanostructures is nowadays categorized in the field of spin caloritronics.[21] Occasionally, the physical origin of the AMR effect is ascribed to spin-dependent scattering ignoring that the symmetry breaking element arises from the spin-orbit interaction.[20] In this context it is interesting to know that in 1999 Ebert *et al.* saw an upcoming trend in the literature to connect the AMR with the giant magnetoresistance and the colossal magnetoresistance.[7] To emphasize the quite different physical origin of these effects they used the name "spontaneous magnetoresistance anisotropy" instead of AMR.[7]

We have measured the electrical and thermal transport properties of individual Ni nanowires as a function of the applied magnetic field in the temperature range between 78 and 300 K. Similar to the AMR effect, we observe an anisotropy of the thermal resistance that in the following will be called anisotropic magnetothermal resistance (AMTR) effect. Investigating the thermal conductivity requires accurate temperature measurements and control over heat generation and heat flow. Our experimental technique is based on the so-called 3ω method that has widely been used for determining the thermal properties of bulk materials,[22] thin films,[23] and suspended wires.[16,24] The characteristic heat diffusion lengths for 3ω measurements range from 100 μm for bulk materials and thin films, to a few micrometers for nanowires. Due to the small length scale, the 3ω method is insensitive to background thermal leakages caused by radiation.[22] Likewise, the corresponding time scales are short, of the order of 1 μs for the Ni nanowire device employed in our work. This is advantageous for observing the AMTR effect. Moreover, in the case of suspended wires, simultaneous measurements of the resistance of the wire, in principle, allows for the direct measurement of the field dependence of the Lorenz number.

The AMR and AMTR effects can be quantified using AMR and AMTR ratios. We define the ratios to be

$$\frac{\Delta R}{R^{\perp}} = \frac{R^{\parallel} - R^{\perp}}{R^{\perp}}; \quad \frac{\Delta W}{W^{\perp}} = \frac{W^{\parallel} - W^{\perp}}{W^{\perp}}, \tag{1}$$

where $R^{\parallel}$ ($R^{\perp}$) is the electrical resistance and $W^{\parallel}$ ($W^{\perp}$) is the thermal resistance at saturation fields applied parallel (perpendicular) to the wire axis; ΔR denotes the absolute AMR; and ΔW denotes the absolute AMTR. Before we discuss the experiment and present the results, we describe the AMTR effect in terms of a simple model that is developed in analogy to the AMR effect. To explain our measurement results, we recapitulate basic knowledge on the AMR effect.

II. ANISOTROPIC MAGNETOTHERMAL RESISTANCE

Most of the theoretical models on AMR are based on the two-current *s-d* scattering model.[25] This model separates the current into a contribution from majority-spin electrons with a resistivity ρ_M and a contribution from minority-spin electrons with a higher resistivity $\rho_m > \rho_M$. The spin-orbit interaction gives rise to mixing or hybridization of the two spin subsystems that causes anisotropic scattering probabilities, for example, of majority spin electrons into minority spin states.[2–7] This mechanism results in a difference $\Delta\rho = \rho^{\parallel} - \rho^{\perp}$ between the resistivities parallel and perpendicular to the spontaneous magnetization. Although the semiclassical models are not rigorous, they provide intuitive understanding of the AMR effect. Campbell *et al.*[3] assumed that ρ_m is solely due to *s-d* scattering arising form isotropic scattering potentials. They considered spin mixing due to electron-magnon scattering by using the spin-flip parameter ρ_{sf}.[26] The AMR ratio is given by[3]

$$\frac{\Delta\rho}{\rho^{\perp}} = \gamma \frac{(\rho_m - \rho_M)\rho_m}{\rho_M\rho_m + \rho_{\mathrm{sf}}(\rho_M + \rho_m)}, \qquad \rho_\sigma = \rho_\sigma^0 + \rho_\sigma^\nu(T), \qquad \sigma \in \{m, M\}, \tag{2}$$

where γ is a constant that is related to the spin-orbit coupling constant, ρ^0 is the residual resitivity, and ρ^ν is the resistivity due to electron-phonon scattering. According to this model, the temperature dependence of the AMR ratio is due to inelastic scattering: electron-magnon scattering that tends to equalize the spin-dependent resistivities, and electron-phonon scattering that is characterized by a different spin asymmetry compared to the scattering at disordered magnetic impurities ($\alpha^0 \equiv \rho_m^0/\rho_M^0 \neq \rho_m^\nu/\rho_M^\nu \equiv \alpha^\nu$).

For ferromagnetic alloys, it was suggested that the main origin of the temperature dependence of the AMR ratio lies in an anisotropic scattering potential for electron-phonon scattering.[27] It was shown by Smit that for nonspherical scattering potentials arising from phonons, grain boundaries, and nonmagnetic impurities, the anisotropy of the transition probability is reduced compared to the transition probability arising from disordered magnetic impurities.[2] Therefore, the AMR ratio decreases as the number of phonons rises, and thus as the temperature rises. In this case the following expression allows for determining the different AMR ratios originating from electron-impurity scattering and from electron-phonon scattering:[27,28]

$$\frac{\Delta\rho}{\rho^\perp}(T) = \left(\frac{\Delta\rho}{\rho^\perp}\right)_{\mathrm{ph}} + \left[\left(\frac{\Delta\rho}{\rho^\perp}\right)_{\mathrm{im}} - \left(\frac{\Delta\rho}{\rho^\perp}\right)_{\mathrm{ph}}\right]\frac{\rho^\perp(0)}{\rho^\perp(T)}, \quad (3)$$

where $\rho^\perp(0) = \rho_{\mathrm{im}}^\perp$ is the residual resistivity at zero temperature. While experimental data on ferromagnetic alloys follow the behavior predicted by Eq. (3), the situation is different for pure ferromagnets. There, due to the lack of magnetic impurities, electron scattering at grain boundaries and phonons lead to a small AMR ratio with a weak temperature dependence.[2] In this case, electron-magnon scattering is required to explain the weak decrease of AMR, which is typically observed at high temperatures.

A thermal analog of the two-current model has recently been proposed by Heikkilä *et al.*[29,30] Within this spin-dependent heat model the two spin channels are characterized by spin-dependent thermal conductivities and temperatures. Assuming a homogeneous ferromagnet (no spin-dependent temperature), the AMTR ratio is given by the equivalent expression of Eq. (2), replacing electrical resistivities by thermal resistivities:

$$\frac{\Delta w}{w^\perp} = \gamma\frac{(w_m - w_M)w_m}{w_M w_m + w_{\mathrm{sf}}(w_M + w_m)}. \quad (4)$$

In contrast to Campbell *et al.*[3], who described ferromagnetic alloys, we assume that all spin-dependent scattering is intrinsically caused by the spin-polarized band structure of pure Ni. Therefore, we assume that all scattering mechanisms j are characterized by the same asymmetry parameter:

$$\alpha^j = \frac{\rho_m^j}{\rho_M^j} = \frac{w_m^j}{w_M^j} \equiv \alpha. \quad (5)$$

The equality between electrical and thermal resistance ratios in this equation is tantamount to the assumption that the Lorenz number $L^j = \rho^j/(w^j T)$, where T is the temperature, is solely determined by the nature of the scattering mechanism j, and thus equal for both spin subsystems. Inserting Eq. (5) into Eqs. (2) and (4) we obtain

$$\frac{\Delta\rho}{\rho^\perp} = \gamma\frac{\alpha(\alpha-1)}{\alpha + \frac{\rho_{\mathrm{sf}}}{\rho_M}(1+\alpha)}, \quad (6)$$

$$\frac{\Delta w}{w^\perp} = \gamma\frac{\alpha(\alpha-1)}{\alpha + \frac{w_{\mathrm{sf}}}{w_M}(1+\alpha)}. \quad (7)$$

If the major contribution to ρ_{sf} and w_{sf} comes from inelastic electron-magnon scattering, it can be expected that $\rho_M/w_M > \rho_{\mathrm{sf}}/w_{\mathrm{sf}}$. To summarize, the simple model developed above suggests two hypotheses: (i) there is an AMTR effect in ferromagnetic conductors due to the spin-orbit interaction, and (ii) in the presence of electron-magnon scattering the AMTR ratio is smaller than the AMR ratio.

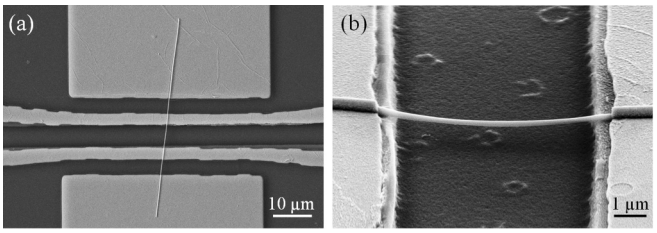

FIG. 1. Scanning electron micrographs of the microdevice used for 3ω measurements on individual nanowires. (a) Top view of a Ni wire with a diameter of 210 nm that is suspended over a trench and connected to four platinum electrodes. (b) Side view of a Ni wire with a diameter of 250 nm that is suspended over a trench (tilt angle: 70° with respect to the substrate normal). The depth of the trenches between the inner contacts is 1 μm.

III. EXPERIMENT

Nickel wires with diameters between 100 and 300 nm and lengths of $\sim$50 μm were grown by electrodeposition in porous alumina membranes.[31] The wires are polycrystalline with an average grain size of $\sim$30 nm, as determined by x-ray diffraction on bundles of nanowires from the same batch. Figure 1 shows scanning electron micrographs of the microdevice employed for 3ω measurements. The device includes a Ni nanowire and four metal electrodes with ohmic contacts to the nanowire. Thermal isolation from the substrate is achieved by suspending the nanowire over a micrometer-sized trench. The specimen is connected to the measurement apparatus using a cryogenic probe station (LakeShore EMPX) that contains an electromagnet for applying horizontal fields up to 550 mT over a temperature range between 8 and 400 K. To avoid heat loss through convection the sample chamber is evacuated to pressures less than 5×10^{-5} mbar. Below we present results on three nanowires. Diameters and lengths of the suspended segment of the nanowires were determined using scanning electron microscopy. These values are summarized in Table I. Small contact resistances were achieved using rf

TABLE I. Geometrical properties of the nanowires investigated.

Wire number	Diameter (nm)	Suspended length (μm)
NW1	160 ± 10	5.8 ± 0.1
NW2	180 ± 10	5.5 ± 0.1
NW3	210 ± 10	5.8 ± 0.1

sputter etching with Ar gas to remove the native nickel oxide shell, directly before sputter deposition of the contact materials (4 nm Ti and 150 nm Pt). By comparing four probe measurements with pseudo four probe measurements, we confirmed that the contact resistances were negligible. The outer contacts are used to inject an alternating current at frequency 1ω into the nanowire that generates Joule heat at frequency 2ω. Due to the temperature-dependent resistivity of the nanowire, the temperature oscillation leads to a resistance oscillation at frequency 2ω that modulates the voltage measured between the inner contacts. The third harmonic component of this voltage, $U_{3\omega}$, is proportional to the amplitude of the temperature oscillation and therefore contains information about the thermal properties of the nanowire.[22,24] The heating current at frequency 1ω is generated using the voltage output of a lock-in amplifier (Stanford Research Systems SR830) in combination with a 10 kΩ resistor. Due to imperfections, the voltage output contains a small component at frequency 3ω that generates a current at frequency 3ω. Furthermore, it is possible that besides the specimen, other time-varying resistances are included in the circuit that contribute to this spurious 3ω current.[32,33] Across the resistance of the specimen, the spurious 3ω current generates a spurious 3ω voltage that contributes to the measurement signal. To obtain the pure 3ω voltage that arises from the temperature oscillations of the specimen, we determined the spurious 3ω voltages at each temperature by measuring the 3ω current using a heat sunk 10 Ω precision resistance that has a negligible temperature coefficient. The precision resistance is connected in series with the specimen. The amplitude of the 3ω voltage measured is typically of the order of 50 μV. The amplitude of the spurious 3ω voltage is of the order of 1–5 μV. The phase difference between the two signals is 180°, i.e., the amplitude of the pure 3ω voltage is obtained by adding both amplitudes. Given by the length of the suspended part of the wire (∼5 μm) the characteristic time of the heat diffusion process is of the order of 1 μs. The output frequency was 277 Hz; whence, the 3ω measurements are performed in the low-frequency limit where the thermal resistance is given by[24,32]

$$W(H) = \frac{48U_{3\omega}(H)}{R(H)\frac{dR(H)}{dT}I^3}, \tag{8}$$

where R is the resistance of the suspended part of the nanowire, and d/dT denotes the temperature derivative; I is the amplitude of the applied current. In this equation we have indicated that besides $W(H)$, also $R(H)$ and $dR(H)/dT$ are functions of the applied magnetic field strength H. As a consequence, the heating and sensing properties of the device change in the presence of magnetic fields. To consider this we measured simultaneously the 3ω and the 1ω components of the voltage signal across the nanowire using two lock-in amplifiers (Stanford Research Systems SR830). Figures 2(a) and 2(b) show representative curves of $U_{3\omega}(H)$ and $U_{1\omega}(H)$ for fields applied perpendicular and parallel to the wire axis, measured at a temperature of 240 K. A comparison of the field dependence of $U_{3\omega}(H)$ and of $U_{1\omega}(H)$ at different temperatures is given in the Supplemental Material.[34,35] The field dependence of $R(H)$ follows directly from $U_{1\omega}(H) = R(H)I$. The field dependence of $dR(H)/dT$ can, in principle, be determined from the consecutive measurements of $R(H)$ at different temperatures. It was shown by Wegrowe *et al.* that the field dependence of $dR(H)/dT$ arises from two terms.[36] The first term considers the temperature variation of the absolute AMR, ΔR, and the second term is due to the thermal susceptibility of the magnetization.[36] At this point we should emphasize that with our work we aim to describe and observe the AMTR effect that is quantified by the AMTR ratio [Eq. (1)]. The interest of our work is not on the behavior of $W(H)$ during the magnetization reversal process. Therefore, we can focus on the saturation values denoted by $W^{\perp}$, $R^{\perp}$ and $W^{\parallel}$, $R^{\parallel}$ for saturation fields applied perpendicular and parallel to the wire

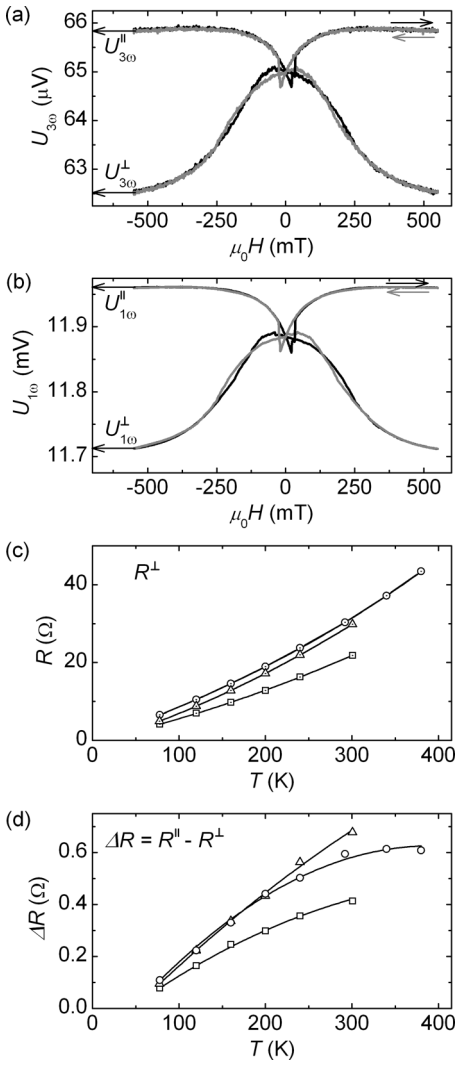

FIG. 2. (a) and (b) Field dependence of the third harmonic (a) and the first harmonic (b) components of the voltage signal at a temperature of 240 K, measured on NW1. The upper (lower) curves show the response to magnetic fields applied parallel (perpendicular) to the wire axis. (c) Temperature dependence of the resistance $R^{\perp}$ at saturation fields applied perpendicular to the wire axis. (d) Temperature dependence of the difference $\Delta R = R^{\parallel} - R^{\perp}$, where $R^{\parallel}$ denotes the resistance at saturation fields applied parallel to the wire axis. Circles, triangles, and squares in (c) and (d) indicate data measured on samples NW1, NW2, and NW3, respectively. Solid lines in (c) and (d) are fit curves to the measurement data using polynomial fits.

axis. At saturation fields, $dR^{\parallel}/dT$ is given by[36]

$$\frac{dR^{\parallel}}{dT} = \frac{dR^{\perp}}{dT} + \frac{d\Delta R}{dT}. \tag{9}$$

The temperature dependence of $R^{\perp}$ and of ΔR of samples NW1, NW2, and NW3 are depicted in Figs. 2(c) and 2(d). The graphs include fit curves to the measurement data that were used to determine $dR^{\perp}/dT$ and $d\Delta R/dT$. Due to the fact that the resistivity of Ni has a complicated temperature dependence in the temperature range under consideration,[37] we applied polynomial fits of second order. Inserting Eq. (8) into the second expression of Eq. (1) we can write the AMTR ratio in terms of the measurement quantities:

$$\frac{\Delta W}{W^{\perp}} = \frac{U^{\parallel}_{3\omega} U^{\perp}_{1\omega} \frac{dR^{\perp}}{dT}}{U^{\perp}_{3\omega} U^{\parallel}_{1\omega} \left(\frac{dR^{\perp}}{dT} + \frac{d\Delta R}{dT}\right)}. \tag{10}$$

It can be seen from Fig. 2(d) that the variation of ΔR becomes very small for temperatures between ~300 K and 380 K. Therefore, it is possible to neglect $d\Delta R/dT$ in Eq. (10) in this temperature range. This approximation was also used by Wegrowe *et al.* for determining the thermal susceptibility of the magnetization of Ni nanowires of diameters between 25 and 40 nm.[36] We return to this point when discussing the experimental results on the AMTR ratio.

IV. RESULTS AND DISCUSSION

We commence the presentation of the experimental results with the temperature dependence of the transport properties shown in Fig. 3. Depicted are the electrical resistivity $\rho^{\perp}$ (a), the thermal conductivity $\kappa^{\perp}$ (b), and the Lorenz number $L^{\perp}$ (c), measured at saturation fields applied perpendicular to the wire axes. The usage of the specific quantities in (a) and (b) allows for the comparison of our results with literature values on bulk Ni,[38] which are plotted in the same graphs. As expected from the polycrystalline nature of the nanowires investigated, $\rho^{\perp}$ is larger and $\kappa^{\perp}$ is smaller than the bulk values of Ni (stars) measured by White and Woods.[38] The enhanced residual resistivity is also responsible for the lack of the low temperature peak of the thermal conductivity that is typically observed in pure bulk metals.[39] The Lorenz number can be written in the same form using either specific quantities or nonspecific quantities:

$$L = \rho\kappa/T = R/(WT). \tag{11}$$

Generally, at high temperatures ($T \gg T_{\mathrm{Debye}}$) and at low temperature ($T \to 0$) elastic scattering of electrons predominates, and the Lorenz number of metals approaches the Sommerfeld value of $L_0 \approx 2.45 \times 10^{-8}\ \mathrm{V^2\,K^{-2}}$.[39] A constant L is known as the Wiedemann Franz law. In the intermediate temperature range, deviations from this law are observed due to inelastic scattering of electrons.[39] Figure 3(c) reveals that the determined values of $L^{\perp}$ for samples NW1 and NW3 are in good agreement with the reference bulk values. $L^{\perp}$ of sample NW2 shows some deviation, of which we have no clear explanation. Below 120 K the observed decrease of $L^{\perp}$ is weaker compared to the bulk values due to the larger residual resistivity of the polycrystalline nanowires.

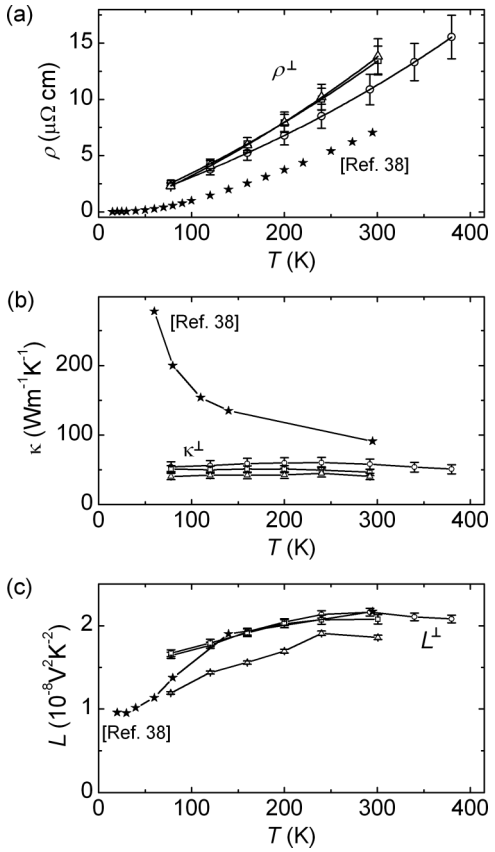

FIG. 3. Temperature dependence of electrical resistivity (a), thermal conductivity (b) and Lorenz number (c) of Ni nanowires, measured under saturation fields applied perpendicular to the wire axes. The bulk values for Ni (stars) were measured by White and Woods (Ref. 38). Circles, triangles, and squares indicate data measured on samples NW1, NW2, and NW3, respectively. Solid lines in (a) are fit curves to the measurement data using polynomial fits. Solid lines in (b) and (c) are guides to the eye.

The results on the AMTR effect, namely, the AMTR ratios defined in Eq. (10), are plotted against the temperature in Fig. 4. The error bars shown were calculated considering Gaussian error propagation of the standard deviations of $U_{3\omega}$, $U_{1\omega}$, $dR^{\perp}/dT$, and $d\Delta R/dT$. A quantitative comparison of the different contributions to the total error is given in the Supplemental Material.[40] As discussed in Sec. III it is possible to neglect the dominant contribution arising from the standard deviation of $d\Delta R/dT$ for temperatures above ~300 K. This would result in a reduction of the error shown in Fig. 4 by a factor of ~5. For comparison we present the corresponding AMR ratios in the same graph. The curves are nonmonotonic with maxima at temperatures between 160 and 200 K. To explain the reduced AMR ratios at low temperatures, we can use Eq. (3) and consider electron-defect scattering instead of electron-impurity scattering:

$$\frac{\Delta\rho}{\rho^{\perp}}(T) = \left(\frac{\Delta\rho}{\rho^{\perp}}\right)_{\mathrm{ph}} + \left[\left(\frac{\Delta\rho}{\rho^{\perp}}\right)_{\mathrm{def}} - \left(\frac{\Delta\rho}{\rho^{\perp}}\right)_{\mathrm{ph}}\right]\frac{\rho^{\perp}(0)}{\rho^{\perp}(T)}, \tag{12}$$

where $(\frac{\Delta\rho}{\rho^{\perp}})_{\mathrm{def}}$ is the AMR ratio due to electron-defect scattering. If $(\frac{\Delta\rho}{\rho^{\perp}})_{\mathrm{def}} < (\frac{\Delta\rho}{\rho^{\perp}})_{\mathrm{ph}}$, Eq. (12) predicts that the

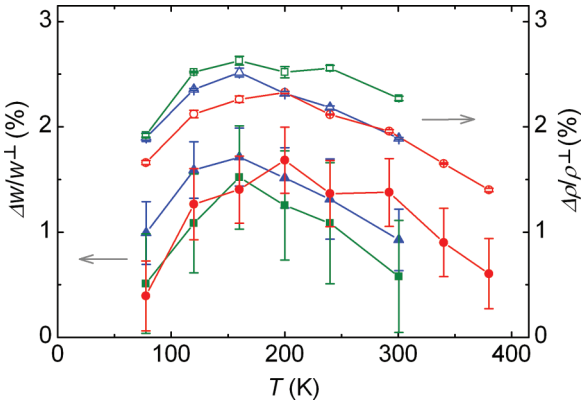

FIG. 4. (Color online) Temperature dependence of the AMR ratio (open symbols) and the AMTR ratio (solid symbols) of Ni nanowires. Red circles, blue triangles, and green squares indicate data measured on samples NW1, NW2, and NW3, respectively. Solid lines are guides to the eye.

AMR ratio increases as the temperature rises, before it saturates at temperatures where electron-phonon scattering dominates. A further effect that can cause a reduction of the AMR ratio at low temperatures is the Lorentz deflection of electrons due to the internal field $B = \mu_0 M_S$, where M_S is the saturation magnetization.[27,41] The decrease of the AMR ratio at higher temperatures can be explained by electron-magnon scattering, using the model of Campbell *et al.*[3] [Eq. (2)]. The AMTR ratios are smaller than the AMR ratios, which is in agreement with the prediction of the simple model presented in Sec. II. The inequality of the AMR and AMTR ratios results in an anisotropic Lorenz number. However, we have to point out that the total thermal conductance that is measured contains isotropic contributions, for example, from phonons. Electrons contribute about 90% to the total thermal conductance in Ni wires with radii above 150 nm.[42] Therefore, we expect that the corrected AMTR ratios would still be well below the AMR ratios.

V. CONCLUSION

We measured the field-dependent electrical and thermal transport properties of individual Ni nanowires in the temperature range between 78 and 380 K. In analogy to the AMR effect observed in ferromagnetic conductors, we found that the thermal resistance of Ni nanowires depends on the angle between magnetization vector and current direction. This anisotropic magnetothermal resistance effect turned out to be weaker than the AMR effect in Ni nanowires over the temperature range investigated. As a consequence, also the Lorenz number was found to be anisotropic with respect to the magnetization direction. Using a simple model, we proposed that spin mixing due to electron-magnon scattering is responsible for this observation. To extend the studies on AMTR we suggest similar measurements on nanowires from ferromagnetic alloys.

ACKNOWLEDGMENTS

We thank S. Martens and D. Görlitz for discussions, and R. Meissner and L. Akinsinde for technical support. This work was supported by the German science foundation (DFG) within the German priority program SPP 1538, "Spin-Caloric Transport".

*johannes.kimling@physik.uni-hamburg.de

[1] W. Thomson, Proc. R. Soc. London **8**, 546 (1857).
[2] J. Smit, Physica **16**, 612 (1951).
[3] I. A. Campbell, A. Fert, and O. Jaoul, J. Phys. C **3**, S95 (1970).
[4] O. Jaoul, I. A. Campbell, and A. Fert, J. Magn. Magn. Mater. **5**, 23 (1977).
[5] T. R. McGuire and R. I. Potter, IEEE Trans. Magn. **11**, 1018 (1975).
[6] J. Banhart and H. Ebert, Europhys. Lett. **32**, 517 (1995).
[7] H. Ebert, A. Vernes, and J. Banhart, Solid State Commun. **113**, 103 (1999).
[8] J.-E. Wegrowe, S. Gilbert, D. Kelly, B. Doudin, and J.-P. Ansermet, IEEE Trans. Magn. **34**, 903 (1998).
[9] J.-E. Wegrowe, D. Kelly, A. Franck, S. E. Gilbert, and J.-P. Ansermet, Phys. Rev. Lett. **82**, 3681 (1999).
[10] S. Pignard, G. Goglio, A. Radulescu, L. Piraux, S. Dubois, A. Declémy, and J. L. Duvail, J. Appl. Phys. **87**, 824 (2000).
[11] Y. Rheem, B.-Y. Yoo, W. P. Beyermann, and N. V. Myung, Nanotechnology **18**, 015202 (2007).
[12] M. Bolte, M. Steiner, C. Pels, M. Barthelmeß, J. Kruse, U. Merkt, G. Meier, M. Holz, and D. Pfannkuche, Phys. Rev. B **72**, 224436 (2005).
[13] M. Hayashi, L. Thomas, C. Rettner, R. Moriya, X. Jiang, and S. S. P. Parkin, Phys. Rev. Lett. **97**, 207205 (2006).
[14] M. V. Kamalakar, A. K. Raychaudhuri, X. Wei, J. Teng, and P. D. Prewett, Appl. Phys. Lett. **95**, 013112 (2009).
[15] M. V. Kamalakar and A. K. Raychaudhuri, Phys. Rev. B **79**, 205417 (2009).
[16] M. N. Ou, T. J. Yang, S. R. Harutyunyan, Y. Y. Chen, C. D. Chen, and S. J. Lai, Appl. Phys. Lett. **92**, 063101 (2008).
[17] B. L. Zink, A. D. Avery, R. Sultan, D. Basser, and M. R. Pufall, Solid State Commun. **150**, 514 (2010).
[18] J.-E. Wegrowe, Q. A. Nguyen, M. Al-Barki, J.-F. Dayen, T. L. Wade, and H.-J. Drouhin, Phys. Rev. B **73**, 134422 (2006).
[19] R. Mitdank, M. Handwerg, C. Steinweg, W. Töllner, M. Daub, K. Nielsch, and S. F. Fischer, J. Appl. Phys. **111**, 104320 (2012).
[20] A. D. Avery, M. R. Pufall, and B. L. Zink, Phys. Rev. B **86**, 184408 (2012).
[21] G. E. W. Bauer, E. Saitoh, and B. J. van Wees, Nature Mater. **11**, 391 (2012).
[22] D. G. Cahill, Rev. Sci. Instrum. **61**, 802 (1990).
[23] D. G. Cahill, M. Katiyar, and J. R. Abelson, Phys. Rev. B **50**, 6077 (1994).
[24] L. Lu, W. Yi, and D. L. Zhang, Rev. Sci. Instrum. **72**, 2996 (2001).
[25] A. P. Malozemoff, Phys. Rev. B **34**, 1853 (1986).
[26] A. Fert, J. Phys. C **2**, 1784 (1969).

[27]L. Berger, P-P-Freitas, J. D. Warner, and J. E. Schmidt, J. Appl. Phys. **64**, 5459 (1988).
[28]R. Parker, Proc. Phys. Soc. London, Sect. A **64**, 447 (1951).
[29]T. T. Heikkilä, M. Hatami, and G. E. W. Bauer, Phys. Rev. B **81**, 100408(R) (2010).
[30]A. Slachter, F. L. Bakker, and B. J. van Wees, Phys. Rev. B **84**, 174408 (2011).
[31]K. Nielsch, F. Müller, A.-P. Li, and U. Gösele, Adv. Mater. **12**, 582 (2000).
[32]C. Dames and G. Chen, Rev. Sci. Instrum. **76**, 124902 (2005).
[33]J. Kimling, S. Martens, and K. Nielsch, Rev. Sci. Instrum. **82**, 074903 (2011).
[34] See Supplemental Material at http://link.aps.org/supplemental/10.1103/PhysRevB.87.094409 for the field dependence of the first and third harmonic components of the measurement signal at different temperatures.
[35]J. J. M. Franse and G. de Vries, Physica **39**, 477 (1968).
[36]J.-E. Wegrowe, Q. A. Nguyen, and T. L. Wade, IEEE Trans. Magn. **46**, 866 (2010).
[37]D. A. Goodings, Phys. Rev. **132**, 542 (1963).
[38]G. K. White and S. B. Woods, Philos. Trans. R. Soc. London, Ser. A **251**, 273 (1959).
[39]C. Uher, in *Thermal Conductivity of Metals*, edited by T. M. Tritt (Kluwer Academic/Plenum Publishers, New York, 2004).
[40] See Supplemental Material at http://link.aps.org/supplemental/10.1103/PhysRevB.87.094409 for a quantitative comparison of the different contributions to the total error of the AMTR ratio.
[41]L. Berger and A. R. de Vroomen, J. Appl. Phys. **36**, 2777 (1965).
[42]N. Stojanovic, D. H. S. Maithripala, J. M. Berg, and M. Holtz, Phys. Rev. B **82**, 075418 (2010).